Revisiting the structures and energies of silicon ⟨110⟩ symmetric tilt grain boundaries

Liang Wang[1], Wenshan Yu[1,a)] ⓘ **, Shengping Shen[1,b)]**

[1]State Key Laboratory for Strength and Vibration of Mechanical Structures, Shaanxi Engineering Laboratory for Vibration Control of Aerospace Structures, School of Aerospace Engineering, Xi'an Jiaotong University, Xi'an 710049, People's Republic of China
a)Address all correspondence to these authors. e-mail: wenshan@mail.xjtu.edu.cn
b)e-mail: sshen@mail.xjtu.edu.cn

Atomistic simulations of 18 silicon ⟨110⟩ symmetric tilt grain boundaries are performed using Stillinger Weber, Tersoff, and the optimized Modified Embedded Atom Method potentials. We define a novel structural unit classification through dislocation core analysis to characterize the relaxed GB structures. GBs with the misorientation angle θ ranging from 13.44° to 70.53° are solely composed of Lomer dislocation cores. For GBs with θ less than but close to 70.53°, GB 'step' appears and the equilibrated states with lowest GB energies can be attained only when such GB 'step' is located in the middle of each single periodic GB structure. For the misorientation angles in the range of 93.37° ≤ θ ≤ 148.41°, GB structures become complicated since they contain multiple types of dislocation cores. This work not only facilitates the structural characterization of silicon ⟨110⟩ STGBs, but also may provide new insights into mirco-structure design in multicrystalline silicon.

Introduction

Multicrystalline silicon (mc-Si) has found wide applications in the fields of solar cells and various electronic devices as thin film transistors due to its relatively low production cost and high performance. The presence of grain boundaries (GBs) in mc-Si can drastically affects its thermodynamic, mechanical [1], and electrical properties [2]. For example, the electrical properties of mc-Si depend on individual GB characters and distributions of GBs [3, 4, 5, 6]. Such properties can be significantly dominated through dopant segregation [7] and interactions between GBs and transition metal impurities [8, 9, 10, 11] by affecting the recombination activity of GBs. Therefore, knowledge of local structures in GBs at the atomic level is essential for better understanding of the electronic characteristics and phase stability of mc-Si and manipulating these properties with the aim to enhance cell performance efficiency.

So far, considerable effort has been dedicated to experimental [12, 13] and theoretical [14, 15, 16, 17] studies of silicon GBs. In fact, experimental characterization shows that various GB misorientations exist in mc-Si, and most GBs are asymmetric. These general and asymmetric GBs are strongly related to the family of symmetric GBs. However, experimental

technique usually cannot systematically help us reveal the structures as well as the energetic properties of symmetric GBs. Thus, researchers resort to the modeling simulations. The first systematic studies of Si GBs are contributed by Kohyama et al. [18, 19] using the bond orbital model [20, 21]. In their studies, sixteen ⟨110⟩ symmetric tilt GBs (STGBs) were investigated. They found that the structures of some low-angle GBs contain Lomer dislocation cores. Besides, some structural units (SUs) [22], composed of 5-, 6-, 7-ring structures, were introduced to geometrically characterize the equilibrated structures of Si STGBs.

Subsequent to Kohyama et al.'s work, more and more studies concentrated on simulations related to silicon GBs. These studies can be generally divided into two categories. One is employing the first-principles method. For example, atomic and electronic structures [23, 24] and their influences on the defect segregations [25] of symmetric and asymmetric GBs such as Σ3, Σ5, and Σ9 were investigated. However, such method can solely deal with small-size model and is incapable of simulating GBs with larger Σ values (the reciprocal coincidence site density). The other is by molecular dynamics (MD) simulations. For example, silicon [001] STGBs were investigated using the harmonic Keating potential [26] and the

environment-dependent tight-binding potential [27]. Besides, asymmetric Σ9 [28] and twist GBs [29] in silicon have been calculated using Stillinger and Weber [30] (SW) and Tersoff [31] potentials. Obviously, these studies do contribute a lot in understanding the structural properties of Si GBs, but are less systematic and basically deal with few Si GBs in comparison to Kohyama et al.'s work.

Till now, three popular empirical potentials, i.e., SW [30], Tersoff [31], and the optimized MEAM [32], developed for silicon have found wide applications in MD simulations. These potentials are based on different theoretical frameworks and may predict different properties of GBs. Some attempts of comparing three potentials have been made, for example, for single Si crystal [33] and few GBs [28, 34]. These studies indeed revealed the material property difference predicted by different potentials, but we are still lacking a thorough understanding of potential influences on silicon ⟨110⟩ STGBs such as structures and energies. This motivates us to ask what influences the three aforementioned potentials have on the energetics and equilibrated structures of silicon ⟨110⟩ STGBs. In addition, Kohyama et al. realized that some silicon ⟨110⟩ STGBs contain the Lomer dislocation core (7–5 rings), but did not analyze whether and how other GB structures are connected with the Lomer dislocation and other types of dislocations. Therefore, another motivation of this study is how to characterize the structures of silicon ⟨110⟩ STGBs using SUs derived from dislocation core structures.

In this study, we attempt to investigate the energetics and equilibrated structures of silicon ⟨110⟩ STGBs by means of three potentials. SUs based on the dislocation core structures are defined to characterize and analyze the GB structures. Then, the detailed atomic structures and energies of eighteen STGBs are analyzed. Finally, remarkable potential dependence of the energies and equilibrated structures of the studied GBs is discussed.

Simulation methodology

Eighteen STGBs with misorientation angle θ ranging from 13.44° to 148.41° are investigated in this study. The reciprocal coincidence site density Σ of all STGBs varies from Σ3 to Σ73. The bicrystal model is constructed with periodic boundary conditions (PBCs) applied within the GB plane, as illustrated in Fig. S10 of Supplementary material. Two grains (i.e., Grains A and B) terminate with free surfaces in the direction perpendicular to the GB plane. Crystalline orientations of two grains and dimensions of computational models for 18 GB are listed in Tables SII and SIII of Supplementary material. All simulations in this study are performed using LAMMPS [35]. Atomic structures are visualized using Ovito [36].

To attain the equilibrated GB structures, we adopt Tschopp et al.'s approach [37], which includes rigid body translations (RBTs) between two grains within GB plane, atoms removing, and statics minimization. The translation increments in the x and y directions are given using the displacement shift complete (DSC) lattice [38]. Meanwhile, atoms in GB that are unphysically too close are removed by using different atomic distance criteria varying from 0.4 to 1.8 Å. The above operations produce hundreds of different configurations for each STGB. Using the conjugate gradient (CG) method [39], these GB configurations are relaxed. Comparing their GB energies, the equilibrated GB state with lowest energy can be obtained. The GB energy γ_{GB} is computed as the total excess potential energies $\left(\sum \left(E^i - E^{Coh} \right) \right)$ of atoms in the slab centered on the GB divided by GB area A_{GB}, i.e., $\gamma_{GB} = \sum \left(E^i - E^{Coh} \right)/A_{GB}$, where E^{Coh} is the cohesive energy (-4.3366 eV/atom for SW, -4.6304 eV/atom for Tersoff and -4.630 eV/atom for MEAM) and E^i is the potential energy of each atom in the slab. The slab thickness is taken as 60 Å. In this way, not only are the effects of free surfaces excluded but also are imperfect effects due to GB included.

Three typical dislocations, i.e., Lomer dislocation, $a[100]$ edge dislocation, and 90° partial dislocation lying on (100), (110), and (111) planes, respectively, are considered for purpose of analyzing GB structures. To generate these dislocations in a perfect silicon crystal, we firstly introduce the Volterra dislocation displacement fields [40] for each type of dislocation at specified sites in the crystal (details see Sec. S1 of Supplementary material). Dislocation structures can be obtained upon relaxation. The Burgers vectors of dislocations are identified by drawing Burgers circuits [40, 41, 42] following RH/FS convention [43].

Results

Analysis of dislocation structures in silicon

Figure 1(a) displays the generated Lomer dislocation core composed of 5- and 7-ring as highlighted in gray, well consistent with the experimental observation [44]. From Fig. S11(a) in Supplementary material, the bond shared by the 5- and 7-ring does not connect in the initial unrelaxed structure. The formation process of this bond undergoing the relaxation is shown in Supplementary material Video S1. The corresponding Burgers vector $\mathbf{b_L}$ is $a[0\bar{1}1]/2$.

In fact, it will be seen that an isolated Lomer dislocation is actually the basic SU of GBs with lower angles. However, as misorientation angle increases, some adjacent Lomer dislocations usually stack together. Here we take the structures of two stacked Lomer dislocations as an example. From Fig. 1(b), the initial unrelaxed structure [Fig. S11(b) in Supplementary material] evolves into a structure composed of 5-, 6-, and
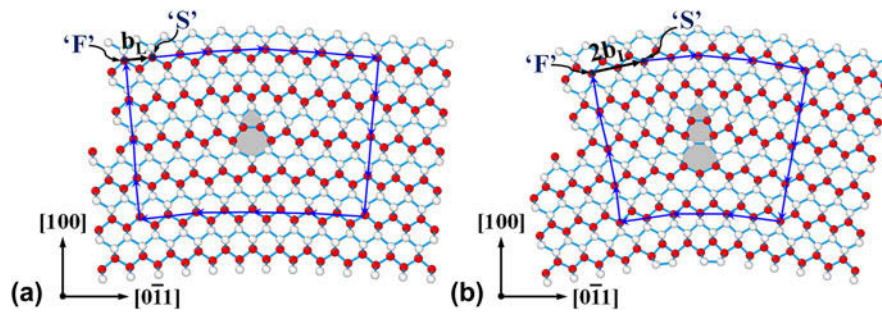
Figure 1: Atomic structures of (a) Lomer dislocation and (b) two adjacent Lomer dislocations. Burgers vector b_L is $a[0\bar{1}1]/2$. Burger vector circuit starts from 'S' point and ends at 'F' point throughout this paper.
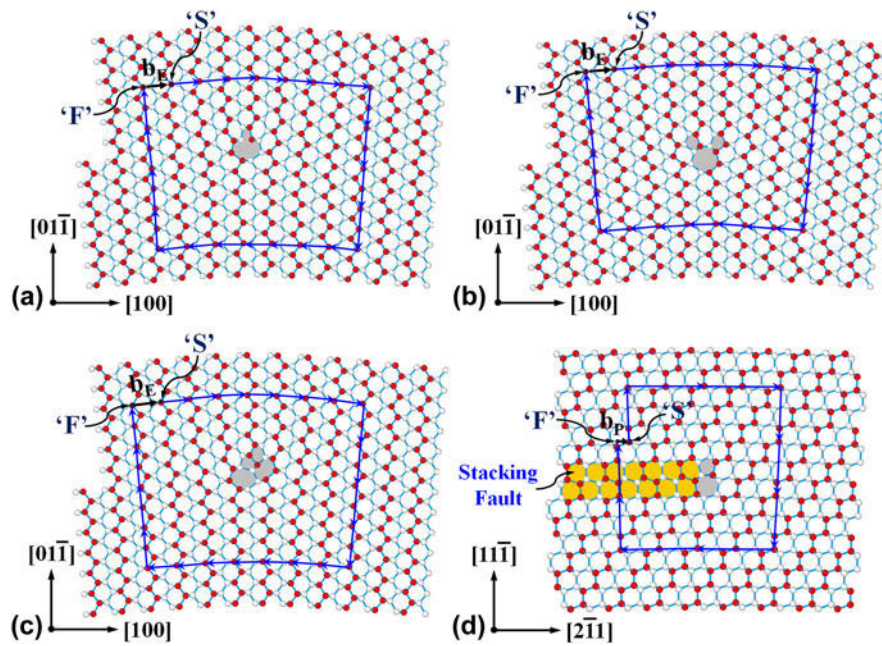

Figure 2: Three different structures of edge dislocation: (a) Edge-I, (b) Edge-II, and (c) Edge-III; and (d) displays the Shockley partial dislocation structure composed of a 7–5-ring core and a trailing stacking fault ribbon. Burgers vector b_E is $a[100]$ and b_p is $a[2\bar{1}1]/6$.

7-ring. The formation process of this structure is shown in Supplementary material Video S2. The corresponding Burgers vector is $2b_L$ $(= a[0\bar{1}1])$. Comparing Figs. 1(a) and 1(b), a 6-ring actually corresponds to a single Lomer dislocation. Later, such a special 6-ring will be proved as the basic SU of twin boundary. As more Lomer dislocations stack together like dislocation wall, the final relaxed structure will exhibit the sequence of 5-, 6-, ..., 6-, and 7-ring.
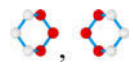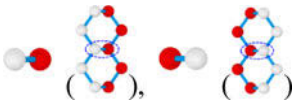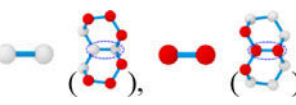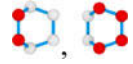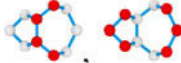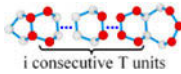
Unlike Lomer dislocation, the structure of $a[100]$ edge dislocation is sensitive to the initial positions for placing Volterra dislocation displacement field such as O_1, O_2, and O_3 (see Fig. S12 in Supplementary material). Three corresponding configurations are denoted as Edge-I, Edge-II, and Edge-III, respectively [Figs. 2(a)–2(c)]. Note that Edge-III is analogous to that constructed by Kohyama et al. [19]. They have the identical Burgers vector b_E $(=a[100])$. Besides, the single-period core structure of 90° partial dislocation with

Burgers vector b_p of $a[2\bar{1}1]/6$ is generated as well, as shown in Fig. 2(d), which is well consistent with the corresponding core reconstruction established by Valladares et al. [45, 46] and Choo et al. [47]. Its core is composed of 5- and 7-ring. The stacking fault (SF) ribbon is bounded by the partial dislocation and the left surface of crystal.

GB structure analysis (13.44° ≤ θ ≤ 70.53°)

Table I shows six SUs for characterizing GBs with $13.44° \leq \theta \leq 70.53°$. SU C^0 constitutes the perfect Si crystal viewing along [110] direction. Two C^0 SUs with coplanar or nonplanar adjoining Si atoms produce SUs C^1 and C^2, respectively. SU T composes the twin boundary. SU L^0 represents the core structure of Lomer dislocation. When two more Lomer dislocations stack together within GB, the local GB structure shows as sequences of 5- and 7-ring separated by some T SUs, as schematically shown

TABLE I: Definition of six structural units (SUs). Atoms on two consecutive (220) planes are colored in red and gray throughout this paper. (For interpretation of the references to color in this table legend, the reader is referred to the web version of this article.)

SU	Atomic structure	Comment
C^0		Perfect crystal
C^1		Two C^0 SUs share a bond with two Si atoms on two consecutive (220) planes
C^2		Two C^0 SUs share a bond with two Si atoms on the same (110) plane
T		Twin boundary unit (equivalent to one Lomer dislocation)
L^0		One Lomer dislocation
L^i	i consecutive T units	$(i + 1)$ Lomer dislocations ($i = 1$ –6)

in Table I. As discussed in section "Analysis of dislocation structures in silicon", a T SU corresponds to a Lomer dislocation. Then, we define SU L^i ($i > 0$) to represent local structure of some GBs containing $(i + 1)$ Lomer dislocations.

For comparison, Table SIV in Supplementary material lists all SUs defined by Kohyama et al. [18]. In their definition, the SU 'T' composing the twin boundary is called boat-shaped 6-membered ring, while SUs 'C' to 'H' are intuitively described as inserting different numbers of SU 'T' into a 7–5 unit (i.e., SU 'B') in succession. By contrast, our defined SUs have the same structural form as Kohyama et al.'s; however, we further demonstrate that SU 'T' corresponds to a single Lomer dislocation while SU 'L^{ib}' ($1 \leq i \leq 6$) consists of $(i + 1)$ Lomer dislocation cores through Burgers vector analyses (see Sec. S2 in Supplementary material). From this perspective, our defined SUs for GBs with misorientation angles $13.44° \leq \theta \leq 70.53°$ are all related to the Lomer dislocation, but Kohyama et al.'s are not. Indeed, Kohyama et al.'s SUs are capable of describing GB structures considered herein. However, it is definitely possible that 'L^{ib}' ($i > 6$) will appear in GBs with misorientation angles $58.99° \leq \theta \leq 70.53°$. In that case, more new SUs are needed if employing the methods of Kohyama et al. to characterize Si GB structures. Clearly, this can be avoided if using our defined SUs.

Using the SUs defined in Table I, we could easily characterize the structures of STGBs with misorientation angles $13.44° \leq \theta \leq 70.53°$. Table II displays the SU descriptions and energies of twelve silicon STGBs. For each GB, we only show

SU description of single periodic GB structure, and the complete GB structures are displayed in Fig. S13 of Supplementary material. For comparison, SU descriptions following Kohyama et al.'s approach are also listed in Table II. In addition, a few intermediate structures with slightly larger energies are also given for GBs $\Sigma33(441)$, $\Sigma9(221)$, $\Sigma11(332)$, $\Sigma41(443)$, and $\Sigma33(554)$.

A preliminary inspection of Table II reveals that three potentials calculate the same structures for all investigated GBs, but different GB energies. For GBs with smaller misorientation angles, their structures only contain SUs C^0, C^1, and L [1]. As misorientation angle gradually increases, the number of C^0 and C^1 in SU description decreases, and C^0 and C^1 vanish for $\theta \geq 55.88°$ [i.e., $\Sigma41(443)$]. In addition, SUs T and L^i ($i > =1$) start to emerge at $\theta = 38.94°$ [i.e., $\Sigma9(221)$]. In particular, for the equilibrated GB states, the angle $38.94°$ [i.e., $\Sigma9(221)$] is a transition misorientation angle. Namely, before and after such misorientation angle, C^0 and C^1 vanish in GB structures and T emerges.

The above analysis indicates that structures of all GBs including their equilibrated and intermediate states can be described by SUs defined in Table I. Therefore, all GB structures in this misorientation range are solely composed of Lomer dislocations. To demonstrate this, we further perform a total Burgers vector analysis by drawing the enclosed Burgers circuits in some GBs (see Sec. S2 in Supplementary material). Following the general theory of GB [40], the Lomer dislocation density in GBs should monotonically increase as misorientation angle increases from $13.44°$ to $70.53°$, as evidenced in Fig. S14 of Supplementary material.

For GBs $\Sigma33(441)$, $\Sigma9(221)$, $\Sigma11(332)$, $\Sigma41(443)$, and $\Sigma33(554)$, the total number of Lomer dislocations in each state is equal, but their energies differ. Note that the equilibrated structures with lowest energies can be obtained only when the GB 'step' appears in the middle of single periodic GB structures. To demonstrate this, we analyze the variations of excess potential energy and hydrostatic stress in states I, II, and IV of $\Sigma11(332)$ GB, calculated with SW potential. From Fig. 3 (a), the maximum excess potential energies in states I, II, and IV are 0.209 eV, 0.169 eV, and 0.151 eV, respectively. Obviously, the excess potential energy of state IV along the x direction is the smallest. From Figs. 3(b) and 3(c), the tensile and compressive stresses decrease a lot in state IV compared to two other counterparts and agree well with Refs. 48 and 49. This implies that significant bond distortion occurs to maintain the straight arrangement of SUs or two closer neighboring 'steps', but bond distortion relaxes when 'step' appears and uniformly distributes within the GB plane [see Fig. 3(c)].

A detailed comparison of our results with those of previous work is shown in Table SV in Supplementary material. It is worth pointing out that our results for GBs $\Sigma33(441)$, $\Sigma9(221)$,

TABLE II: SU descriptions and energies for the twelve silicon GBs with misorientation angles $13.44° \leq \theta \leq 70.53°$. The minimum GB energies calculated with three potentials for each GB are highlighted in red. (For interpretation of the references to color in this table legend, the reader is referred to the web version of this article.)

| θ	GB		'SU' description	Structure arrangement	GB energy [J/m^2]		
					SW	Tersoff	MEAM
13.44°	Σ73(661)		$L^0(C^1C^0)_2C^1L^0C^1C^0C^1$ (BAABA)[a]		**0.594**	**0.185**	**0.726**
16.1°	Σ51(551)		$(L^0C^1C^0C^1)_2$ (BABA)[a]		**0.587**	**0.183**	**0.715**
20.05°	Σ33(441)	I	$(L^0C^1)_2C^0C^1$ (BBA)[a]		0.634	0.198	0.767
		II	$L^0C^0C^1L^0C^1C^0$		**0.598**	**0.187**	**0.721**
26.53°	Σ19(331)		$L^0C^1L^0C^1$ (B.B)[a]		**0.505**	**0.160**	**0.604**
31.59°	Σ27(552)		$(L^0)_3C^1L^0C^1$ (BB'B.B)[a]		**0.593**	**0.180**	**0.707**
38.94°	Σ9(221)	I	C^1L^1 (C)[a]		0.862	0.276	1.059
		II	$(L^0)_2$ (BB')[a]		**0.453**	**0.134**	**0.526**
44.0°	Σ57(774)		$C^1(L^1L^0)^2L^1$ (CB'CB'C)[a]		**0.712**	**0.221**	**0.858**
45.98°	Σ59(553)		$(L^0L^1)_2$ (BC'BC')[a]		**0.604**	**0.187**	**0.718**
50.48°	Σ11(332)	I	C^1L^3 (E)[a]		1.055	0.333	1.301
		II	L^0L^2 (BD')[a]		0.696	0.216	0.832
		III	$L^1(L^0)^2$		0.641	0.200	0.766
		IV	$(L^1)_2$ (CC')[a]		**0.618**	**0.193**	**0.741**
55.88°	Σ41(443)	I	L^0L^4 (BF')[a]		0.763	0.237	0.919
		II	L^1L^3 (CE')[a]		0.666	0.210	0.804
		III	$(L^2)_2$ (DD')[a]		**0.638**	**0.202**	**0.766**
58.99°	Σ33(554)	I	L^0L^6 (BH')[a]		0.756	0.237	0.908
		II	L^1L^5 (CG')[a]		0.669	0.209	0.807
		III	L^2L^4 (DF')[a]		0.630	0.203	0.756
		IV	$(L^3)^2$ (EE')[a]		**0.620**	**0.20**	**0.743**
70.53°	Σ3(111)		T_2		**0**	**0**	**0**

[a]SU descriptions taken from Ref. 18.
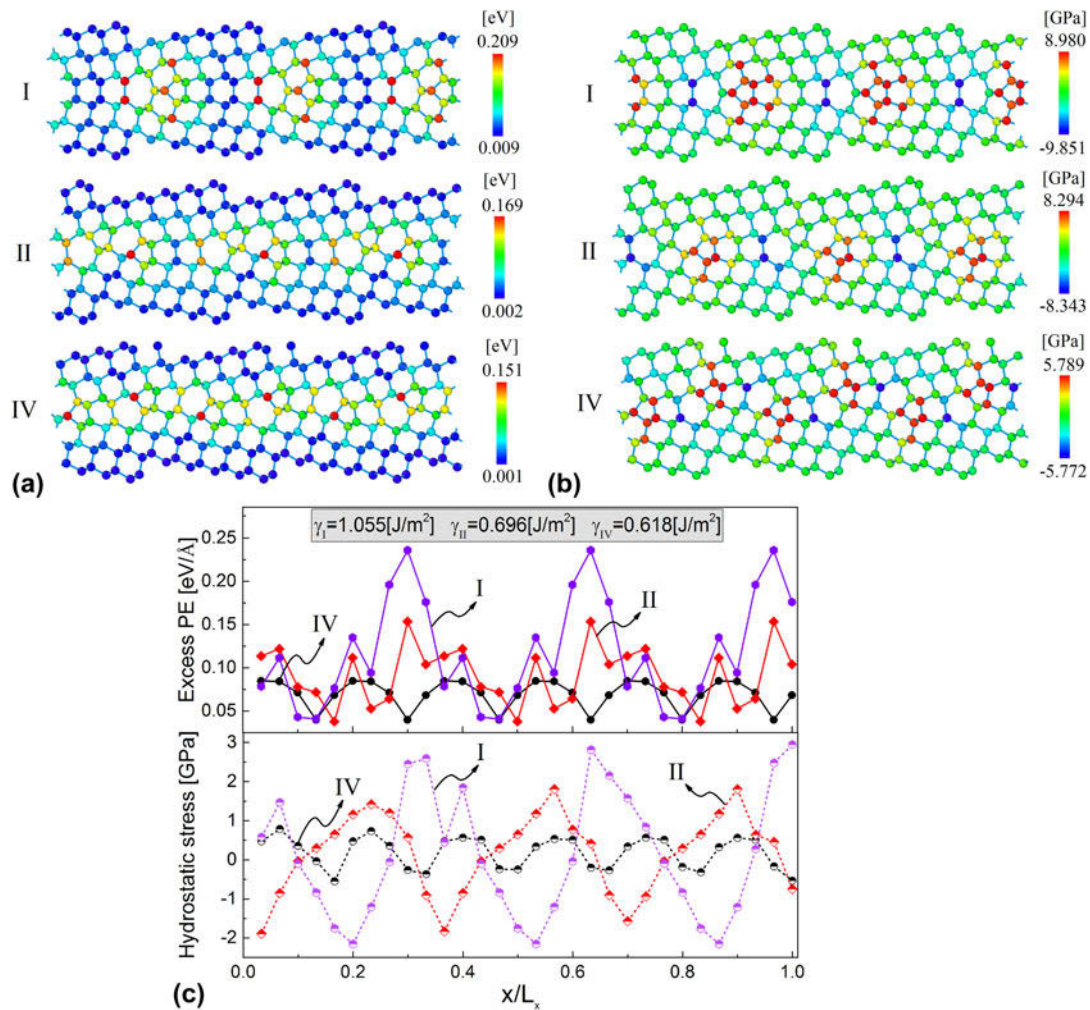
Figure 3: The distributions of (a) excess potential energy (PE) and (b) hydrostatic stress of I, II, and IV states for Σ11(332) GB calculated with SW potential. (c) The variations of excess potential energy and hydrostatic stress versus normalized x position. Calculation details are given in Sec. S3 in Supplementary material. (For interpretation of the references to color in this figure legend, the reader is referred to the web version of this article.)

and Σ11(332) calculated with SW and Tersoff potentials are in good agreement with those in Refs. 50, 51, and 52. Additionally, our calculated GB structures in the misorientation angle range $13.44° \leq \theta \leq 70.53°$ exclude any coordination defects or dangling bonds, well consistent with the experimental and computational results. For example, the atomic structures for GBs Σ51(551), Σ33(441) (state I), Σ19(331), Σ27(552), Σ9 (221), Σ59(553), Σ11(332) (state IV), and Σ41(443) (state III) agree well with those proposed by Kohyama et al. [18]. For GBs Σ73(661), Σ57(774), Σ11(332) (states I and II), Σ41(443) (states I and II), and Σ33(554), Koyhama et al. only predicted the structural arrangement but did not provide the corresponding atomic structures and energies. For these GBs, we not only calculate the predicted GB structures but also determine the equilibrated structure for each GB with three potentials. Moreover, the structure of Σ33(441) GB (state II) has been experimentally observed in Ref. 50.

GB structure analysis (93.37° ≤ θ ≤ 148.41°)
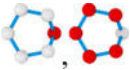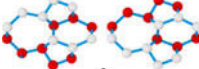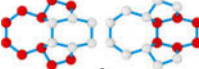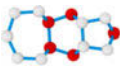
Table III lists twelve representative SUs to describe six silicon ⟨110⟩ STGBs with misorientation angles $93.37° \leq \theta \leq 148.41°$. SU 'S' is a special 6-ring found only in GBs with θ larger than 93.37°. SU 'P' represents the core structure of 90° Shockley partial dislocation [Fig. 2(d)]. SUs 'E^I' and 'E^{II}' are the two different core structures of a[100] edge dislocation [Figs. 2(a) and 2(b)]. 'E$^{I/S}$' and 'E$^{II/S}$' are obtained by shearing 'E^I' and 'E^{II}' along the x direction by the length of each core structure. SU 'F$^0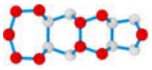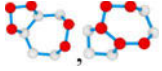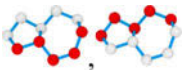$' is composed of 7–5 ring, whose Burgers vector is $2/3[2\bar{1}1]a$ equivalent to four 90° Shockley partials (see Fig. S15 in Supplementary material). Similar to the definition of SU L^i in Table I, SUs F^1 and F^2 can be viewed as the SU F^0 with one and two T SUs inserted. As for SUs A and B^1, they are another two new 7–5 rings. SU B^2 can be recognized as a structure transformed from SU B^1 by rotating the 5-membered ring a certain angle. Clearly, most SUs in Table III have definite

interpretation. To facilitate comparison, those SUs defined by Kohyama et al. [19] consisting of isolated 5-, 6-, and 7-ring are listed in Table SVI in Supplementary material.

Table IV displays the single periodic structures and energies calculated with three potentials for six silicon STGBs with $93.37° \leq \theta \leq 148.41°$. The complete structures of these GBs are shown in Fig. S16 in Supplementary material. Using our defined SUs in Table III and those by Kohyama et al. [19] in Table SVI in Supplementary material, each GB structure is described. Clearly, our approach simplifies a lot the characterization of GB structures.

Besides, some intermediate structures with larger energies are given for all GBs except $\Sigma33(225)$ GB. Unlike those GBs with $\theta \leq 70.53°$, GB structures shown in Table IV differ markedly and comprise rather different SUs. The energies of all six STGBs for three potentials are also shown in Table IV, with the minimum GB energies in red. From Table IV, any GB can find its lowest energy corresponding to the specific potential apart from $\Sigma33(225)$ GB. For $\Sigma33(225)$ GB, the single periodic GB structure shown in Table IV is the most stable for MEAM, but not for SW and Tersoff. The calculated GB structures with minimum energies of 1.008 J/m^2 for SW and 0.772 J/m^2 for Tersoff are displayed in Fig. 4, respectively.

TABLE III: Definitions of SUs for STGBs with misorientation angles $93.37° \leq \theta \leq 148.41°$. (For interpretation of the references to color in this table legend, the reader is referred to the web version of this article.)

SU	Atomic structure	SU	Atomic structure
S	(Special 6-ring)	P	(One partial)
E^I	(Edge-I)	E^{II}	(Edge-II)
E$^{I/S}$	(Sheared Edge-I)	E$^{II/S}$	(Sheared Edge-II)
F^0	(Four partials)	F^1	(Four partials + T)
F^2	(Four partials + 2T)	A	
B^1		B^2	

Comparing Tables II and IV, the energies of GBs with $93.37° \leq \theta \leq 148.41°$ are much larger than those with $13.44° \leq \theta \leq 70.53°$. This can be attributed to the presence of co-ordination defects or large bond distortions spreading along the GBs with $\theta \geq 93.37°$. For example, we calculate two different structures for $\Sigma3(112)$ GB, i.e., states I (mirror-symmetric) and II (asymmetric). Although they are both consistent with the experimental observations [53, 54, 55] and theoretical calculations [56, 57, 58], they contain under- or over-coordinated atoms. Specifically, state I contains dangling bonds and both symmetric and asymmetric structures contain 5-fold coordinate atoms from our results. However, atoms in GBs with $13.44° \leq \theta \leq 70.53°$ are all 4-fold coordinated. This explains why GBs with $93.37° \leq \theta \leq 148.41°$ have larger energies.

Comprehensive comparison between our results and others' is made for these six GBs (see Table SVII in Supplementary material). For example, the structure of state V for $\Sigma17(223)$ GB shown in Table IV agrees well with the structure description in Ref. 19. The structure of state I of $\Sigma11(113)$ GB coincides well with that proposed by Morris et al. [14, 17, 19]. The state I configuration of $\Sigma9(114)$ GB resembles the atomic model deduced from the experiments [53]. Finally, it is worth noting that the structures of $\Sigma11(113)$ (state II) and $\Sigma27(115)$ (state II) GBs are composed of an array of $a[100]$ edge dislocations.

Discussions

Structures of Si STGBs

In this work, we define some novel SUs connected to the dislocation core structure. These defined SUs simplify the structure characterization of silicon $\langle110\rangle$ STGBs with misorientation angles $13.44° \leq \theta \leq 148.41°$. For GBs with $13.44° \leq \theta \leq 70.53°$, their structures are found to be solely composed of Lomer dislocations. In fact, a Lomer dislocation core simply consists of 5- and 7-membered rings, which was first defined by Kohyama et al. [18, 19] as an SU to characterize some GB structures. Their work also presented some GB structures containing 5- and 7-membered rings with some 6-rings inserted between them, i.e., 7–6,..., 6–5 rings. They just simply define some SUs named from B to I to describe these structures, but fail to unveil what dislocation cores they contain. Our analysis shows that 7–6,..., 6–5 rings actually represent some stacked Lomer dislocations. In addition, the inserted 6-ring corresponds to a single Lomer dislocation. These are demonstrated by our dislocation structure analysis in single Si crystal and Burgers vector analysis in GB (see Sec. S2 in Supplementary material).

For some GBs with $13.44° \leq \theta \leq 70.53°$, we also study their intermediate states with different structures. These states for

TABLE IV: Structural unit descriptions and average energies for six silicon GBs with misorientation angles 93.37° ≤ θ ≤ 148.41°. The lowest GB energies calculated with three potentials for each GB are highlighted in red. (For interpretation of the references to color in this table legend, the reader is referred to the web version of this article.)

θ	GB		'SU' description	Structure arrangement	GB energy [J/m²]		
					SW	Tersoff	MEAM
93.37°	Σ17(223)	I	$C^2F^2\left(\begin{smallmatrix}6^0\\6^0\end{smallmatrix}\,7^06^16^15^1\right)^a$		1.367	0.751	1.299
		II	$F^1P\left(7^06^15^1\,{}_{7^25^0}\right)^a$		1.133	0.422	1.079
		III	$F^1B^2T\left(7^06^15^1\,\begin{smallmatrix}6^1\\7^15^0\end{smallmatrix}\right)^a$		1.084	0.536	**0.952**
		IV	$AT_2A\left(\begin{smallmatrix}5^0\\5^0\end{smallmatrix}\,7^06^16^1\,7^0\right)^a$		0.843	0.254	1.117
		V	$(AT)_2\left(\begin{smallmatrix}5^0\\5^0\end{smallmatrix}\,7^06^1\,7^06^1\right)^a$		**0.753**	**0.251**	0.955
109.47°	Σ3(112)	I	$C^2F^0\left(\begin{smallmatrix}6^0\\6^0\end{smallmatrix}\,7^05^1\right)^a$		1.256	0.961	**0.977**
		II	$SP\left(6^2\,7^25^0\right)^a$		**1.115**	**0.813**	1.711
121.01°	Σ33(225)		$(C^2S)_2C^2F^0\left(\left(\begin{smallmatrix}6^0\\6^0\end{smallmatrix}\,6^2\right)_2,\begin{smallmatrix}6^0\\6^0\end{smallmatrix}\,7^05^1\right)^a$		1.499	1.119	**1.207**
129.52°	Σ11(113)	I	$(C^2S)_2\left(\left(\begin{smallmatrix}6^0\\6^0\end{smallmatrix}\,6^2\right)_2\right)^a$		1.280	0.891	**0.936**
		II	$(E^I)_2$		**1.061**	**0.340**	1.759
		III	$(E^{I/S})_2$		1.161	0.579	1.325
141.06°	Σ9(114)	I	$SC^2SB^1\left(6^2\,\begin{smallmatrix}6^0\\6^0\end{smallmatrix}\,6^25^07^1\right)^a$		1.324	0.901	**1.066**
		II	$E^{II}B^2P$		**0.960**	**0.726**	1.415
148.41°	Σ27(115)	I	$(SB^1)_2\left(\left(6^25^07^1\right)_2\right)^a$		**0.840**	0.883	**0.831**
		II	$(E^{II})_2$		1.115	0.769	1.616
		III	$(E^{II/S})_2$		0.852	**0.393**	1.546

ᵃSU descriptions taken from Ref. 19.

a GB can also be easily described using our defined SUs. The total numbers of Lomer dislocation cores in these intermediate states are equal to the corresponding equilibrated counterpart. The equilibrated state of a GB can be obtained only when the GB step appears in the middle of single periodic structure for GBs Σ11(332), Σ41(443), and Σ33(554). For GBs with 93.37° ≤ θ ≤ 148.41°, their structures are more complex and no significant structural variation trend exists compared to those with 13.44° ≤ θ ≤ 70.53°. But this does not prevent us from identifying the definite physical significance of SUs (Table III) with regard to these GBs and simplifying the characterization of corresponding GB structures (Table IV).

Energies of Si STGBs

Theoretically, there are a vast number of structures for a given GB, originating from its equilibrated state due to the irradiation, plastic deformation, and material fabrication process.
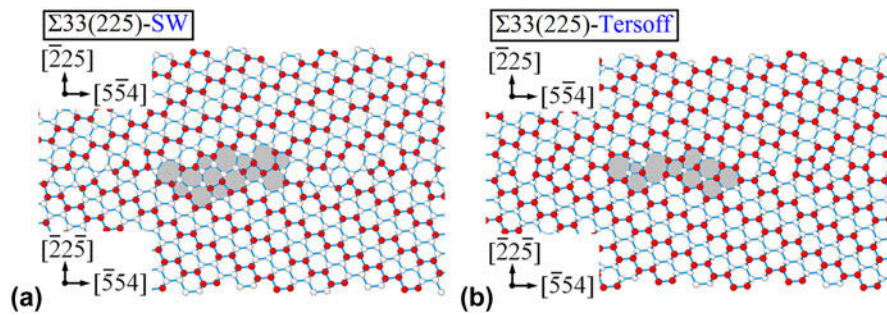
Figure 4: The equilibrated structures of Σ33(225) GB calculated with (a) SW and (b) Tersoff potentials, respectively.

Therefore, it is of great significance to obtain and characterize the equilibrated state of each GB. Generally, a standard commonly used procedure just performs the relaxation and annealing of as-constructed GBs. However, such method is unable to modulate the number of atoms in GB; thus, the equilibrated GB state with the lowest energy cannot usually be obtained, in particular for asymmetric GBs and GBs of some complex crystals. To do so, some approaches have been developed, for example, due to Tschopp et al. [37, 59, 60], Yu and Demkowicz [61], Frolov et al. [62], and Alfthan and Sutton et al. [29, 63] etc. In this study, we adopt Tschopp et al.'s approach to optimize the structures of Si STGBs and obtain their equilibrated states using three potentials.

However, the equilibrated states of some GBs cannot be attained solely by RBTs within the GB plane, and removing atoms within the set cutoff radius, the optimized GB structures may contain dangling bonds. Such dangling bonds are physical unreasonable and mainly related to the truncation of atomic interaction distance of three potentials (see Fig. S6 in Supplementary material). In fact, this may be the intrinsic fault of three potentials. If we deliberately increase the cutoff distances of three potentials, the second nearest neighbor atoms would bond and incorrect bonds may also form in GB and the crystal away from GB. Instead, we displace either side of grains along the GB normal prior to the GB relaxation so that atoms of these dangling bonds in two grains could successfully shake. By implementing such operation, previous GBs with dangling bonds could easily be brought to the states with lower energies (see Sec. S4 in Supplementary material).

Figure 5 plots the energies of equilibrated GBs versus misorientation angle. The energy difference between as-constructed and equilibrated GBs is given in Fig. S17 of Supplementary material, suggesting that the equilibrated structures have much lower energies than the as-constructed for each GB. For comparison, the MD results based on the SW and Tersoff potentials are plotted in Fig. 5, along with the DFT values for certain GBs. A more detailed comparison between our results and others' via other different potentials and methods is made in Tables SV and SVII in Supplementary

material. From Fig. 5, the energies of GBs with $13.44° \leq \theta \leq 70.53°$ are lower than those of GBs with $93.37° \leq \theta \leq 148.41°$ for three potentials. Overall, the energies of GBs with $13.44° \leq \theta \leq 70.53°$ exhibit similar variation trend and vary around ~0.6 J/m^2, ~0.2 J/m^2, and ~0.7 J/m^2 for SW, Tersoff, and MEAM potentials. In fact, this is completely due to the simpler structures of GBs with $13.44° \leq \theta \leq 70.53°$, i.e., only composed of Lomer dislocations. Moreover, energy of each GB for MEAM potential is the largest while that for Tersoff is the smallest. Such is related to the different Lomer dislocation core energies (E_c) calculated by three potentials, as manifested by the linear correlation between the GB energies and the Lomer dislocation core energies [Fig. 6(c)]. Because of complicated structures of GBs with $93.37° \leq \theta \leq 148.41°$, different from GBs with $13.44° \leq \theta \leq 70.53°$, there is no consistent magnitude order of energies for each GB calculated by three potentials.

From Figs. 6(a)–6(c), three potentials calculate the same Lomer dislocation core structure with saturated 4-fold co-ordinated bonds. However, not only the magnitude but also the atom sites of the maximum and minimum potential energies for Tersoff potential are completely different from those for
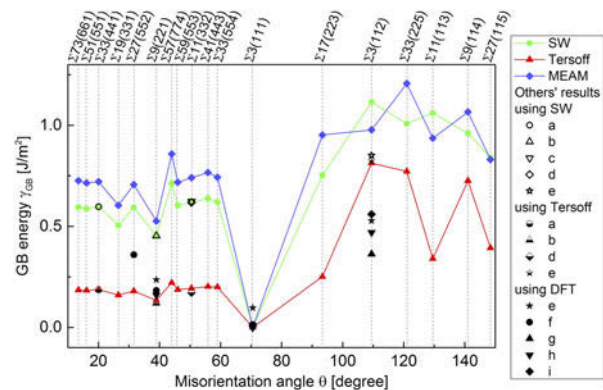

Figure 5: The energies of equilibrated Si⟨110⟩ STGBs versus misorientation angle, calculated with SW, Tersoff, and MEAM potentials. Others' results calculated with SW and Tersoff potentials from studies by [a]Lamzatouar et al. [64], [b]Ihlal et al. [51], [c]Chen et al. [52], and [d]Hardouin Duparc et al. [65] and the DFT values obtained from studies by [e]Stoffers et al. [28], [fg]Zhao et al. [49, 57] [h]Ziebarth et al. [66], and [i]Sakaguchi et al. [67] are also plotted for comparison.
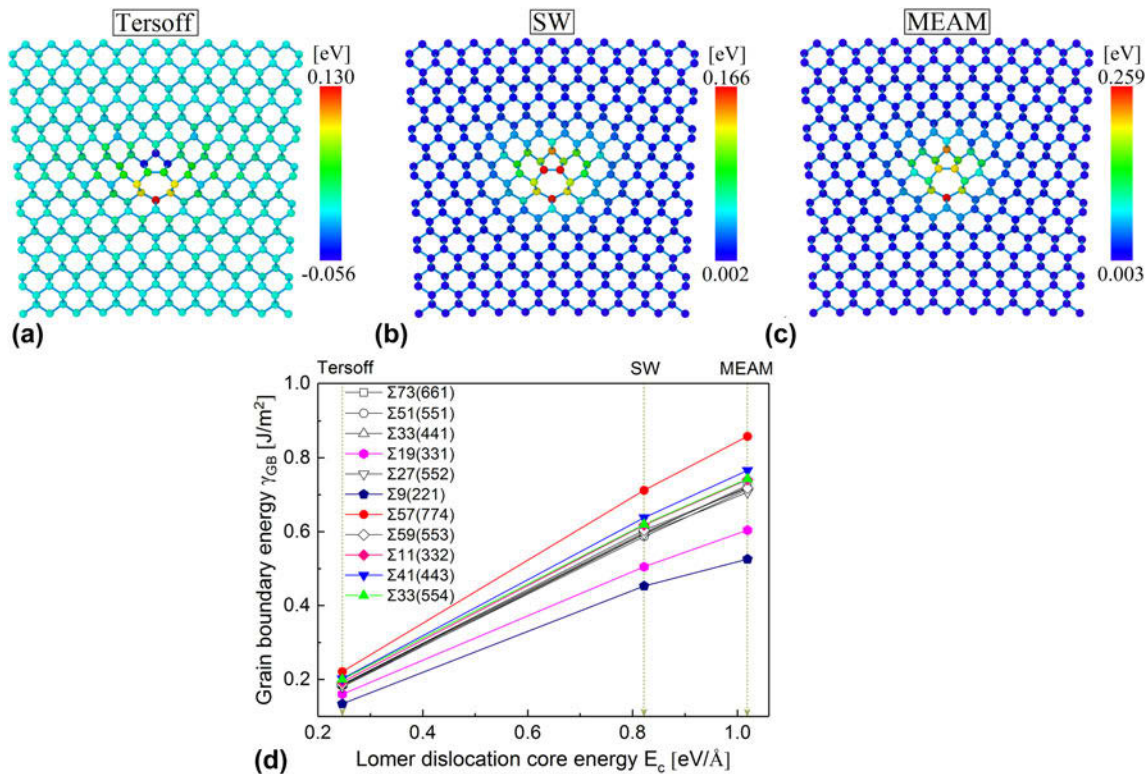
Figure 6: The distributions of excess potential energies around Lomer dislocation core calculated with (a) Tersoff, (b) SW, and (c) MEAM potentials; and (d) displays the GB energies of equilibrated GBs with $13.44° \leq \theta \leq 70.53°$ versus Lomer dislocation core energies. E_c is the total excess potential energy of Si atoms in the circular region with radius 4 times the Burgers vector $(a[0\bar{1}1]/2)$ divided by the length of dislocation line (L_y). E_c are 0.247 eV/Å, 0.822 eV/Å, and 1.019 eV/Å for Tersoff, SW, and MEAM potentials, respectively. (For interpretation of the references to color in this figure legend, the reader is referred to the web version of this article.)

other two potentials. Besides, we also compare the distributions and variations of excess potential energies and hydrostatic stresses of state IV of $\Sigma11(332)$ GB for three potentials (see Sec. S5 in Supplementary material). These together indicate the different descriptions of lattice distortion in terms of bond geometry and GB structure arrangement by three potentials for GBs with misorientations $13.44° \leq \theta \leq 70.53°$. Meanwhile, the potential energy values and distribution around dislocation core predicted by SW potential are analogous to those for MEAM potential by comparing Figs. 6(b) and 6(c). This is actually due to the similar theoretical framework of SW and MEAM potentials [68]. This also accounts for the GB energies and their variation trends of SW potential similar to those of MEAM potential.

We further compare three potentials by analyzing the energies and atomic structures of the relaxed (100), (110), and (111) surfaces and mono-vacancy in Si crystal (see Sec. S6 in Supplementary material). In these structures, the atoms of surfaces and the inner atoms in the vacancy are under-coordinated. Three potentials calculate different surface energies and vacancy formation energies, suggesting the different descriptions of under-coordinated bonds by three potentials. This is in accordance with the statement that the coordination

number appears to be an most important variable influencing the bond order proposed by Tersoff [31]. For GBs with misorientation angles $93.37° \leq \theta \leq 148.41°$, their structures are more complicated than those of GBs with $13.44° \leq \theta \leq 70.53°$. Some coordinate defects (under- and over-coordinated chemical bonds) exist in the GBs. The combined influence of lattice distortion in terms of atom arrangement and bond connection (bond length and angle) as well as coordination number, leads to different descriptions of GB structures and energies by three potentials.

Conclusions

In this study, we study the structures and energies of eighteen silicon $\langle110\rangle$ STGBs using SW, Tersoff and the optimized MEAM potentials. To clearly characterize the structures of these GBs, the core structures of Lomer dislocation, $a[100]$ edge dislocation and 90° Shockley partial dislocation in the perfect Si crystal are analyzed. Based on this, we then introduce some SUs connected to the dislocations to describe the Si GB structures. In addition, we also compare our results with some previous results in terms of GB structure description and energies. To further demonstrate the remarkable potential

dependence of GB energies and structures, the core energies of Lomer dislocation predicted by three potentials are analyzed as well. The main conclusions of this study are drawn as:

(1) For GBs with misorientation angles $13.44° \leq \theta \leq 70.53°$, we find that all their structures including equilibrated and intermediate states can be well described by a collection of Lomer dislocations. This is proved by the analysis of dislocation structure and total Burgers vector in the GB region.

(2) For some GBs with misorientation angle less than but close to $70.53°$, their intermediate structures contain the same number of Lomer dislocation cores. Moreover, the presence of GB 'step' in them seems helpful in reducing the GB energies. Besides, the equilibrated GB structure with lowest GB energy can be attained only when the 'step' locates in the middle of the single periodic structure.

(3) In comparison to GBs with $13.44° \leq \theta \leq 70.53°$, Si STGBs with $93.37° \leq \theta \leq 148.41°$ show complicated structures described by more complex SUs. That is because they contain not only the core structures of a [100] edge dislocation and 90° Shockley partial dislocation along with their variants but also several other different 7–5 rings and a special 6-ring.

(4) Three potentials calculate the same equilibrated structures but different energies for GBs with $13.44° \leq \theta \leq 70.53°$. Whereas for GBs with $93.37° \leq \theta \leq 148.41°$, not only the GB energies but also the energetically favorable GB structures differ for three potentials. This implies that the intrinsic differences between three potentials significantly affect the calculated GB properties, in particular for GBs with $93.37° \leq \theta \leq 148.41°$. Therefore, one should be cautious in selecting an appropriate potential to perform simulations related to Si STGBs.

Acknowledgments

Supplementary material

To view supplementary material for this article, please visit https://doi.org/10.1557/jmr.2018.437.

References

1. S. Bringuier, V.R. Manga, K. Runge, P. Deymier, and K. Muralidharan: An atomic scale characterization of coupled grain boundary motion in silicon bicrystals. *Philos. Mag.* **95**, 4118 (2015).

2. G. Stokkan: Twinning in multicrystalline silicon for solar cells. *J. Cryst. Growth* **384**, 107 (2013).

3. Z. Wang, S. Tsurekawa, K. Ikeda, T. Sekiguchi, and T. Watanabe: Relationship between electrical activity and grain boundary structural configuration in polycrystalline silicon. *Interface Sci.* **7**, 197 (1999).

4. J. Chen, T. Sekiguchi, D. Yang, F. Yin, K. Kido, and S. Tsurekawa: Electron-beam-induced current study of grain boundaries in multicrystalline silicon. *J. Appl. Phys.* **96**, 5490 (2004).

5. J. Chen, T. Sekiguchi, R. Xie, P. Ahmet, T. Chikyo, D. Yang, S. Ito, and F. Yin: Electron-beam-induced current study of small-angle grain boundaries in multicrystalline silicon. *Scr. Mater.* **52**, 1211 (2005).

6. J. Chen and T. Sekiguchi: Carrier recombination activity and structural properties of small-angle grain boundaries in multicrystalline silicon. *Jpn. J. Appl. Phys.* **46**, 6489 (2007).

7. A. Maiti, M.F. Chisholm, S.J. Pennycook, and S.T. Pantelides: Dopant segregation at semiconductor grain boundaries through cooperative chemical rebonding. *Phys. Rev. Lett.* **77**, 1306 (1996).

8. S. Joonwichien, S. Matsushima, and N. Usami: Effects of crystal defects and their interactions with impurities on electrical properties of multicrystalline Si. *J. Appl. Phys.* **113**, 133503 (2013).

9. I. Takahashi, N. Usami, H. Mizuseki, Y. Kawazoe, G. Stokkan, and K. Nakajima: Impact of type of crystal defects in multicrystalline Si on electrical properties and interaction with impurities. *J. Appl. Phys.* **109**, 033504 (2011).

10. O.V. Feklisova, X. Yu, D. Yang, and E.B. Yakimov: Effect of metal contamination on recombination properties of extended defects in multicrystalline Si. *Phys. Status Solidi C* **9**, 1942 (2012).

11. S. Ambigapathy, V. Natarajan Sathiyamoorthy, S. Ryoji, M. Hiroshi, and K. Yoshiyuki: First-principles calculations on Σ3 grain boundary transition metal impurities in multicrystalline silicon. *Jpn. J. Appl. Phys.* **49**, 04DP02 (2010).

12. J.L. Putaux and J. Thibault-Dessaux: HREM characterization of structural changes in a deformed Σ = 9 (122) grain boundary in silicon. *J. Phys. Colloq.* **51**, C1-C323 (1990).

13. J. Thibault, J.L. Putaux, A. Jacques, A. George, H.M. Michaud, and X. Baillin: Structure and characterization of the dislocations in tilt grain boundaries between Σ = 1 and Σ = 3: A high resolution electron microscopy study. *Mater. Sci. Eng., A* **164**, 93 (1993).

14. H.J. Möller: ⟨011⟩ tilt boundaries in the diamond cubic lattice. *Philos. Mag. A* **43**, 1045–1055 (1981).

15. R.E. Thomson and D.J. Chadi: Theoretical study of the electronic structure of a high-angle tilt grain boundary in Si. *Phys. Rev. B* **29**, 889 (1984).

16. **M. Kohyama, R. Yamamoto, Y. Ebata, and M. Kinoshita**: The atomic and electronic structure of a (001) tilt grain boundary in Si. *J. Phys. C: Solid State Phys.* **21**, 3205 (1988).

17. **J.R. Morris, C.L. Fu, and K.M. Ho**: Tight-binding study of tilt grain boundaries in diamond. *Phys. Rev. B* **54**, 132 (1996).

18. **M. Kohyama, R. Yamamoto, and M. Doyama**: Structures and energies of symmetrical ⟨011⟩ tilt grain boundaries in silicon. *Phys. Status Solidi B* **137**, 11 (1986).

19. **M. Kohyama, R. Yamamoto, and M. Doyama**: Reconstructed structures of symmetrical ⟨011⟩ tilt grain boundaries in silicon. *Phys. Status Solidi B* **138**, 387 (1986).

20. **M. Lannoo and J.N. Decarpigny**: Simple tight-binding calculation of the transverse effective charges in III–V, II–VI, and IV–IV compound semiconductors. *Phys. Rev. B* **8**, 5704 (1973).

21. **W.A. Harrison**: *Electronic Structures and the Properties of Solids* (Freeman, San Fransisco, 1980); pp. 26, 43.

22. **A.P. Sutton and V. Vitek**: On the structure of tilt grain boundaries in cubic metals I. Symmetrical tilt boundaries. *Philos. Trans. R. Soc., A* **309**, 1 (1983).

23. **D.P. DiVincenzo, O.L. Alerhand, M. Schlüter, and J.W. Wilkins**: Electronic and structural properties of a twin boundary in Si. *Phys. Rev. Lett.* **56**, 1925 (1986).

24. **W.L. Huang, W. Ge, C.X. Li, C.F. Hou, X.W. Wang, and X.F. He**: Atomic and electronic structures of Si[001] (130) symmetric tilt grain boundaries based on first-principles calculations. *Comput. Mater. Sci.* **58**, 38 (2012).

25. **V.Y. Lazebnykh and A.S. Mysovsky**: Ab initio and atomistic simulation of local structure and defect segregation on the tilt grain boundaries in silicon. *J. Appl. Phys.* **118**, 135704 (2015).

26. **A.A. Levi, D.A. Smith, and J.T. Wetzel**: Calculated structures for [001] symmetrical tilt grain boundaries in silicon. *J. Appl. Phys.* **69**, 2048 (1991).

27. **J. Zhang, C. Wang, and K. Ho**: Finding the low-energy structures of Si[001] symmetric tilted grain boundaries with a genetic algorithm. *Phys. Rev. B* **80**, 174102 (2009).

28. **A. Stoffers, B. Ziebarth, J. Barthel, O. Cojocaru-Miredin, C. Elsasser, and D. Raabe**: Complex nanotwin substructure of an asymmetric Σ9 tilt grain boundary in a silicon polycrystal. *Phys. Rev. Lett.* **115**, 235502 (2015).

29. **S.v. Alfthan, K. Kaski, and A.P. Sutton**: Order and structural units in simulations of twist grain boundaries in silicon at absolute zero. *Phys. Rev. B* **74**, 134101 (2006).

30. **F.H. Stillinger and T.A. Weber**: Computer simulation of local order in condensed phases of silicon. *Phys. Rev. B* **31**, 5262 (1985).

31. **J. Tersoff**: New empirical approach for the structure and energy of covalent systems. *Phys. Rev. B* **37**, 6991 (1988).

32. **M. Timonova and B.J. Thijsse**: Optimizing the MEAM potential for silicon. *Modell. Simul. Mater. Sci. Eng.* **19**, 015003 (2011).

33. **H. Balamane, T. Halicioglu, and W.A. Tiller**: Comparative study of silicon empirical interatomic potentials. *Phys. Rev. B* **46**, 2250 (1992).

34. **J. Narayan and A.S. Nandedkar**: Atomic structure and energy of grain boundaries in silicon, germanium and diamond. *Philos. Mag. B* **63**, 1181 (1991).

35. **S. Plimpton**: Fast parallel algorithms for short-range molecular dynamics. *J. Comp. Physiol.* **117**, 1 (1995).

36. **S. Alexander**: Visualization and analysis of atomistic simulation data with OVITO–the Open Visualization Tool. *Modell. Simul. Mater. Sci. Eng.* **18**, 015012 (2010).

37. **M.A. Tschopp and D.L. McDowell**: Structures and energies of Σ3 asymmetric tilt grain boundaries in copper and aluminium. *Philos. Mag.* **87**, 3147 (2007).

38. **W. Bollmann**: *Crystal Defects and Crystalline Interfaces* (Springer-Verlag, New York, Heidelberg, Berlin, 1970); pp. 186, 214.

39. **D.P. Bertsekas**: *Nonlinear Programming*, 3rd ed. (Athena Scientific, Cambridge, Massachusetts, 2016); pp. 22, 75.

40. **J.P. Hirth and J. Lothe**: *Theory of Dislocations*, 2nd ed. (McGraw-Hill, New York, 1982); pp. 59, 92.

41. **A.P. Sutton and R.W. Balluffi**: *Interfaces in Crystalline Materials* (Clarendon Press, Oxford, 1995); pp. 87, 88.

42. **W. Yu, Z. Wang, and S. Shen**: Edge dislocations interacting with a Σ11 symmetrical grain boundary in copper upon mixed loading: A quasicontinuum method study. *Comput. Mater. Sci.* **137**, 162 (2017).

43. **D. Hull and D.J. Bacon**: *Introduction to Dislocations*, 5th ed. (Butterworth-Heinemann, Oxford, 2011); pp. 14, 20.

44. **A. Bourret, J. Desseaux, and A. Renault**: Core structure of the Lomer dislocation in germanium and silicon. *Philos. Mag. A* **45**, 1 (1982).

45. **A. Valladares, A.K. Petford-Long, and A.P. Sutton**: The core reconstruction of the 90° partial dislocation in silicon. *Philos. Mag. Lett.* **79**, 9 (1999).

46. **A. Valladares and A.P. Sutton**: The equilibrium structures of the 90° partial dislocation in silicon. *J. Phys.: Condens. Matter* **17**, 7547 (2005).

47. **Z.M. Choo, M.H. Liang, and S. Li**: Atomistic simulation of the core structure of 90° partial dislocation in silicon: A Burgers vector perspective. *Key Eng. Mater.* **227**, 151 (2002).

48. **P. Käshammer and T. Sinno**: Interactions of twin boundaries with intrinsic point defects and carbon in silicon. *J. Appl. Phys.* **114**, 083505 (2013).

49. **D. Zhao and Y. Li**: Lattice distortion induced site dependent carbon gettering at twin boundaries in silicon. *J. Alloys Compd.* **712**, 599 (2017).

50. **M. Kohyama, H. Ichinose, Y. Ishida, and M. Nakanose**: Tight-binding calculation of grain boundaries in diamond. *Mater. Sci. Forum* **207–209**, 261 (1996).

51. **A. Ihlal, R. Rizk, and O.B.M. Hardouin Duparc**: Correlation between the gettering efficiencies and the energies of interfaces in silicon bicrystals. *J. Appl. Phys.* **80**, 2665 (1996).

52. **J. Chen, A. Hairie, E. Paumier, and G. Nouet**: Energy of the two variants 11A and 11B in silicon and germanium by the semi-

empirical tight-binding method. *Phys. Status Solidi B* **232**, 191 (2002).

53. **Y.G. Zhang, H. Ichinose, M. Nakanose, K. Ito, and Y. Ishida**: Structure modelling of Σ3 and Σ9 coincident boundaries in CVD diamond thin films. *J. Electron Microsc.* **48**, 245 (1999).

54. **H. Sawada and H. Ichinose**: Structure of {112} Σ3 boundary in silicon and diamond. *Scr. Mater.* **44**, 2327 (2001).

55. **K. Masanori**: Computational studies of grain boundaries in covalent materials. *Modell. Simul. Mater. Sci. Eng.* **10**, R31 (2002).

56. **H. Sawada, H. Ichinose, and M. Kohyama**: Gap states due to stretched bonds at the (112) Σ3 boundary in diamond. *J. Phys.: Condens. Matter* **19**, 026223 (2007).

57. **D. Zhao and Y. Li**: Carbon segregation at Σ3 {1$\bar{1}\bar{2}$} grain boundaries in silicon. *Comput. Mater. Sci.* **143**, 80 (2018).

58. **C.B. Feng, J.L. Nie, X.T. Zu, M.M. Al-Jassim, and Y. Yan**: Structure and effects of vacancies in Σ3 (112) grain boundaries in Si. *J. Appl. Phys.* **106**, 113506 (2009).

59. **M.A. Tschopp and D.L. McDowell**: Asymmetric tilt grain boundary structure and energy in copper and aluminium. *Philos. Mag.* **87**, 3871 (2007).

60. **M.A. Tschopp, K.N. Solanki, F. Gao, X. Sun, M.A. Khaleel, and M.F. Horstemeyer**: Probing grain boundary sink strength at the nanoscale: Energetics and length scales of vacancy and interstitial absorption by grain boundaries in α-Fe. *Phys. Rev. B* **85**, 064108 (2012).

61. **W.S. Yu and M.J. Demkowicz**: Non-coherent Cu grain boundaries driven by continuous vacancy loading. *J. Mater. Sci.* **50**, 4047 (2015).

62. **T. Frolov, D.L. Olmsted, M. Asta, and Y. Mishin**: Structural phase transformations in metallic grain boundaries. *Nat. Commun.* **4**, 1899 (2013).

63. **S. Von Alfthan, P.D. Haynes, K. Kaski, and A.P. Sutton**: Are the structures of twist grain boundaries in silicon ordered at 0 K? *Phys. Rev. Lett.* **96**, 055505 (2006).

64. **A. Lamzatouar, M. El Kajbaji, A. Charaï, M. Benaissa, O.B. M. Hardouin Duparc, and J. Thibault**: The atomic structure of Σ = 33{144} ⟨011⟩ (θ = 20.05°) tilt grain boundary in germanium. *Scr. Mater.* **45**, 1171 (2001).

65. **O.B.M. Hardouin Duparc and M. Torrent**: A new type of periodie boundary condition useful for high-temperature atomistic simulations of grain boundaries: Applications in semiconductors. *Interface Sci.* **2**, 7 (1994).

66. **B. Ziebarth, M. Mrovec, C. Elsässer, and P. Gumbsch**: Interstitial iron impurities at grain boundaries in silicon: A first-principles study. *Phys. Rev. B* **91**, 035309 (2015).

67. **N. Sakaguchi, H. Ichinose, and S. Watanabe**: Atomic structure of faceted Σ3 CSL grain boundary in silicon: HRTEM and ab initio calculation. *Mater. Trans.* **48**, 2585 (2007).

68. **B.J. Thijsse**: Relationship between the modified embedded-atom method and Stillinger–Weber potentials in calculating the structure of silicon. *Phys. Rev. B* **65**, 195207 (2002).